Applied Thermal Engineering 117 (2017) 109–121

Contents lists available at ScienceDirect

Applied Thermal Engineering

journal homepage: www.elsevier.com/locate/apthermeng

Research Paper

Effects of clothing and fibres properties on the heat and mass transport, for different body heat/sweat releases

S.F. Neves [a,b], J.B.L.M. Campos [b], T.S. Mayor [b,c,*]

[a] Nanolayer Coating Technologies, LDA, Rua Fernando Mesquita, 2785, 4760-034 Vila Nova de Famalicão, Portugal
[b] Transport Phenomena Research Center (CEFT), Chemical Engineering Department, Engineering Faculty of Porto University, Rua Dr Roberto Frias, 4200-465 Porto, Portugal
[c] Swiss Federal Laboratories for Materials Science and Technology (EMPA), Lerchenfeldstrasse 5, 9014 St. Gallen, Switzerland

HIGHLIGHTS

- Heat/mass transport rates in clothing analysed for several textile/fibre properties.
- Analyses done for different levels of heat/sweat release (exercise & post-exercise).
- Fibre diffusion rate and clothes emissivity affect skin temperature (in exercise).
- Fibre diffusion rate, fraction, density and water affinity affect water content.
- Fibre fraction, density and water affinity affects water content (in post-exercise).

GRAPHICAL ABSTRACT

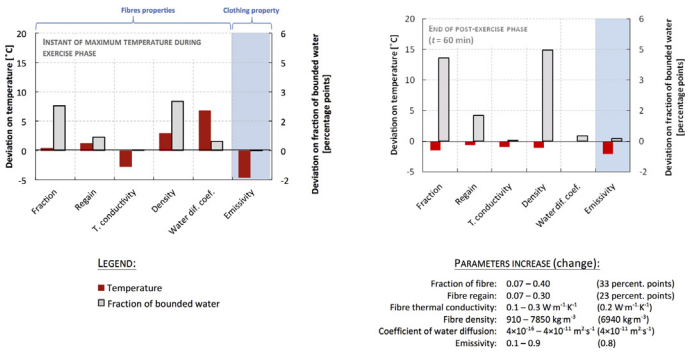

ARTICLE INFO

Article history:
Received 19 May 2016
Revised 25 November 2016
Accepted 21 January 2017
Available online 9 February 2017

Keywords:
Clothing properties
Fibre properties
FEM approach
Simulation
Heat and mass transfer
Physical activity
Sweat production
Water content
Water distribution

ABSTRACT

Clothing plays a key role in the capacity of the body to adapt to the surrounding thermal environments. Thus, it is critically important to have a solid understanding of the effects of clothing and fibres properties on the body exchange rates. To this end, a detailed transfer model was implemented to analyse the effect of several textiles characteristics (outer surface emissivity, tortuosity, and fraction of fibre) and fibre properties (affinity with water, coefficient of water diffusion in the fibres, thermal conductivity, density, and specific heat), on the heat and mass transfer through multilayer clothing, for different intensities of heat/sweat release. The temperature and humidity predictions were validated with experimental data obtained during measurements of textile evaporative resistance.

The results obtained for the multilayer clothing during an energy-demanding activity (i.e. metabolic heat production of 300 W m^{-2} and sweating of 240 g m^{-3} h^{-1}) show that a decrease in the emissivity of the outer surface (0.9 – 0.1), and an increase in the coefficient of water diffusion in the fibres of the inner layer (4×10^{-16} – 4×10^{-11}), induce an increase in the maximum skin temperature (of 4.5 °C and 6.8 °C, respectively). Moreover, the water trapped inside clothing is significantly increased by augmenting the fraction of fibre (0.07 – 0.4), the density of the fibre (910 – 7850 kg m^3), the fibre affinity with water (i.e. regains of 0.07 – 0.3), and the coefficient of water diffusion in the fibres (4×10^{-16} – 4×10^{-11}). During the post-exercise phase (with metabolic heat production of 65 W m^{-2} and perspiration of 9 g m^{-3} h^{-1}), the parameters affecting significantly the water content of the inner layer are the fraction of fibre, its density, and its affinity with water.

* Corresponding author at: Transport Phenomena Research Center (CEFT), Chemical Engineering Department, Engineering Faculty of Porto University, Rua Dr Roberto Frias, 4200-465 Porto, Portugal.
E-mail address: tiago.sottomayor@fe.up.pt (T.S. Mayor).

http://dx.doi.org/10.1016/j.applthermaleng.2017.01.074
1359-4311/

The proposed numerical approach allows the study of strategies to optimise heat/mass transport rates through materials surrounding the body (e.g. in clothing applications, automotive environments or workplace microclimates) in order to minimise thermal discomfort and/or problems of high water content (e.g. friction burns and/or growth of fungi and bacteria).

Nomenclature

a_s	specific surface area [m^{-1}]
A	area [m^2]
C	concentration [kg m^{-3}]
C_p	specific heat [J kg^{-1} K^{-1}]
d	diameter [m]
D_a	diffusivity of water vapour in air [m^2 s^{-1}]
D_{ef}	effective diffusivity of gas through the textile [m^2 s^{-1}]
D_f	diffusivity of water in fibre [m^2 s^{-1}]
f_A	fraction of fibre surface covered by liquid water [–]
h_c	heat transfer coefficient [W m^{-2} K^{-1}]
k_c	mass transfer coefficient [m s^{-1}]
k	thermal conductivity [W m^{-1} K^{-1}]
L	thickness [m]
Le	Lewis number [–]
$\dot{m}_{GS}$	mass rate sorption of water from fibres to the gaseous phase [kg s^{-1} m^{-3}]
$\dot{m}_{LG}$	mass rate of condensation or evaporation of water [kg s^{-1} m^{-3}]
$\dot{m}_{LS}$	mass rate sorption of free water in fibres [kg s^{-1} m^{-3}]
M	molar mass [kg mol^{-1}]
Nu	Nusselt number [–]
p	partial pressure [Pa]
$\dot{q}$	heat flux [W m^{-2}]
r	fibre radius [m]
Pr	Prandtl number [–]
R	gas constant [J K^{-1} mol^{-1}]
$Regain_{eq}$	equilibrium regain [kg_{H2O} kg_{fibre}^{-1}]
$Regain_{f(\varphi=65\%)}$	equilibrium regain for φ = 65% [kg_{H2O} kg_{fibre}^{-1}]
$Regain_t$	instantaneous regain [kg_{H2O} kg_{fibre}^{-1}]
t	time [s]
T	temperature [K]
V	volume [m^3]
x	coordinate [m]

Greek letters

Δh_{sorp}	enthalpy of water desorption from fibre to the liquid phase [J kg^{-1}]
Δh_{vap}	water vaporisation enthalpy [J kg^{-1}]
ε	volume fraction [–]
ε_r	emissivity [–]
ρ	density [kg m^{-3}]
τ	tortuosity [–]
φ	relative humidity [–]
γ_{ls}	proportionality constant for the sorption of liquid water in fibres [kg m^{-3}]
σ	Stefan-Boltzmann constant [W m^{-2} K^{-4}]

Superscripts

cond	condensation
conv	convection
evap	evaporation
ls	liquid - solid
sat	saturation

Subscripts

a	air
amb	ambient
bw	bounded water
ds	dry fibre
ef	effective
GS	gas – solid
LS	liquid – solid
GL	gas – liquid
f	fibre
l	liquid
v	water vapour
T	total
0	initial condition
γ	gas phase
σ	solid phase

1. Introduction

The body adapts the heat exchange in response to changes in the surrounding environment. In a thermally neutral environment, when an individual carries out a moderate activity, the body continuously generates heat and a residual amount of water vapour is excreted by the skin, i.e. insensible perspiration [1–3]. Together with the environmental conditions (e.g. air temperature, humidity, and velocity), the properties of the clothing worn by the user have a crucial role in the heat and mass exchange between the body and the environment. However, when the cooling needs of the body increase (e.g. because of an increase in the intensity of physical activity or in the ambient temperature), the body starts sweating in order to benefit from evaporative cooling, i.e. heat loss due to sweat evaporation. Yet, if the clothing water vapour permeability hampers significantly the sweat transport, the sweat accumulates near the skin (increasing its wetness) and only a portion evaporates. This is often the case in warm working environments or military scenarios, where individuals may sweat for long periods, thus exposing themselves to eventual dehydration and heat stroke. Another detrimental effect of water accumulation in clothing is the resulting tactile discomfort associated with the perception of a wet surface in contact with the skin. Moreover, this increases the risk of skin friction burns during activities implying motion and eventually excessive cooling during post-exercise phase. These drawbacks can be minimised by a good understanding of how clothing properties influence heat and mass transfer from the body. This is critical for the design and development of protective clothing, where the selection of materials must follow accurate criteria to avoid the risk of injuries or even death, with the particular challenge of combining protection (e.g. to chemical agents, thermal hazards) and thermal comfort. This knowledge is also very relevant when developing automotive environments or artificial microclimates for workplaces [4,5].

Several thermal manikins and experimental procedures have been developed to evaluate the performance of different types of products under various conditions [6–11]. Zhao et al. [6] used a thermal manikin to study the influence of design features of a ventilated clothing on cooling performance, while Elabbassi et al. [10] used a similar approach to analyse the efficiency of an electric-heated blanket in preventing hypothermia in neonates. The usual procedure consists of setting constant temperature or heat flux on the manikin surface [6,8–10], corresponding to skin values of an human in a state of thermal comfort. Recently, the surface temperature and sweat rates of some thermal manikins have been controlled by mathematical models of human thermoregulation [7,12,13]. However, few research has focussed on the effect of clothing properties on the surface of the thermal manikin, during consecutive activities with different levels of intensity [11,14]. In these experiments, sequences of different heat fluxes (or temperatures) and sweating rates are imposed on the manikin surface, in order to simulate different human activities. For example, Keiser [11] analysed experimentally the water distribution within a fire-fighter garment, simulating the conditions of a sweating phase followed by a drying phase. Each layer of the garment was weighted at the beginning and at the end of each phase. However, the disadvantage of this procedure is that the results do not show the evolution and distribution of water over the entire experiment. A reliable alternative would be to perform a numerical analysis of the heat/mass transport through the garments.

As in experimental procedures, the skin boundary conditions of heat and of mass are often set constant in numerical studies of heat and mass transfer through clothing [15–24]. Neves et al. [15] studied the thermal performance of multilayer clothing assuming constant temperature and sweat rate on the skin, whereas Wu and Fan [18] defined the mass boundary condition as the concentration of water saturation, when studying a multilayer assembly exposed to a cold ambient. The aforementioned boundary conditions are also used in other field of application like artificial microclimates to study the interaction between the building ventilation and personalised airflow systems, with the thermal plume around human body [25–28]. In clothing applications, those boundary conditions are used to study various design parameters concerning how products properties should be selected to minimise the wind chill effect [19,20,22,29], and how the microclimates inside clothing affect the transport rates from the body [30–33]. However, the available literature still lacks detailed information about parameters of multilayer clothing that affect its thermal performance and water distribution, when the user performs physical activity implying different heat/sweat release.

In this study, numerical simulations were conducted to analyse the effect of several fibre properties (affinity with water, coefficient of water diffusion in the fibre, thermal conductivity, density, and specific heat) and textiles characteristics (outer surface emissivity, tortuosity, and fraction of fibre) on the heat and mass transfer across a textile assembly, during activities implying different levels of heat/sweat release. A 1-D approach was used considering: (i) an external boundary (representing the external clothing surface) exposed to ambient air, where heat is removed by forced convection and radiant exchange while mass is removed by convection; (ii) an inner boundary (representing the skin-clothing interface) where two values of heat flux and water vapour flux were considered in order to mimic the heat/sweat released by the body, during activities with two levels of intensity.

2. Formulation of the transfer model

2.1. Model assumptions and equations

In order to approximate a realistic scenario, the performance of a multilayer clothing was studied for different levels of heat/sweat release (Fig. 1). Three phases were considered: phase 0 corresponding to the acclimatization period, followed by a phase of exercise (phase I, Fig. 1) and a post-exercise phase (phase II, Fig. 1). Throughout the simulation, the environment conditions of temperature, relative humidity, and air velocity were assumed constant (20 °C, 40%, and 0.5 m s^{-1}, respectively). At the initial time (t = 0 s, Fig. 1), the subject was assumed to be in equilibrium with the environment, with a constant temperature of 34 °C and a constant perspiration rate of 9 g m^{-3} h^{-1} (i.e. insensible perspiration, [1–3]). In the subsequent phase, the subject performs a physically-intensive activity, represented by high heat flux and high sweat rate during 30 min, followed by a resting period of 30 min, with low heat flux and no sweating (only perspiration). During phases I and II, two scenarios may occur depending on the amount of water (vapour or liquid) released by the skin. While the rate of sweat production is smaller than the maximum rate that can be transferred through the clothing (i.e. when both perspiration and sweating may be present but the skin is not fully wet; Fig. 2a), one assumes that the total amount of water released by the skin evaporates and the resulting vapour diffuses through the clothing layer. When the rate of sweat production is bigger than the maximum rate that can be transferred by diffusion through the clothing (i.e. when the skin becomes fully wet or saturated; Fig. 2b), one assumes that there is dripping of excess water and that the boundary condition at the skin is well represented by the concentration of saturated water vapour.

To represent the thermal behaviour of the multilayer clothing during the different phases of exercise (Fig. 1), the numerical model considers the heat transferred by conduction and the enthalpies of sweat vaporisation, as well as those of water sorption/desorption in fibres and the diffusion of water vapour across the clothing porous network (Fig. 2).

The implemented model describes the transient diffusion of heat and mass through hygroscopic materials, following the general governing equations given by Le et al. [34,35], Barker et al. [36], and Gibson [37]. The model considers that the textile contains three elements (fibres, air with water vapour and liquid water), and the major simplifying assumptions are: (1) the textile material is considered a homogeneous medium with mentioned three elements (i.e. the complex structure of the material is not taken into account), (2) the liquid water is sorbed at the fibres surface (i.e. there is no motion of liquid water across the layers), (3) heat transfer by radiation between fibres is negligible, (4) the sorption/desorption of water from fibres occurs by water diffusion through the fibre, (5) the water diffusion in the fibre is instantaneous and at the initial rate, (6) water sorption occurs exclusively in the area of fibres which is not in contact with free water, and (7) water

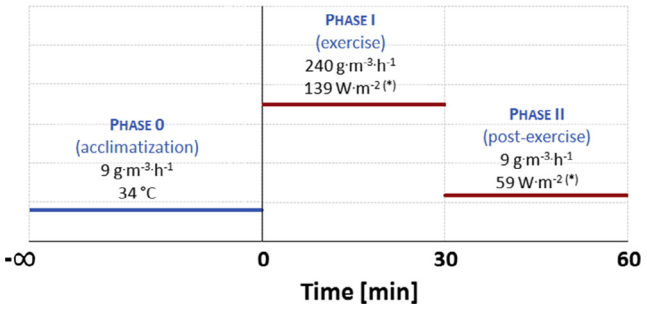

Fig. 1. Physical activity phases used to study the performance of a multilayer clothing; heat and mass boundary conditions defined at the skin-clothing surface for three phases: acclimatization, exercise, and post-exercise; * Difference between metabolic heat production (phase I: 300 W m^{-2}; phase II: 65 W m^{-2}) and the heat removal by sweat evaporation (phase I: 161 W m^{-2}; phase II: 6 W m^{-2}).

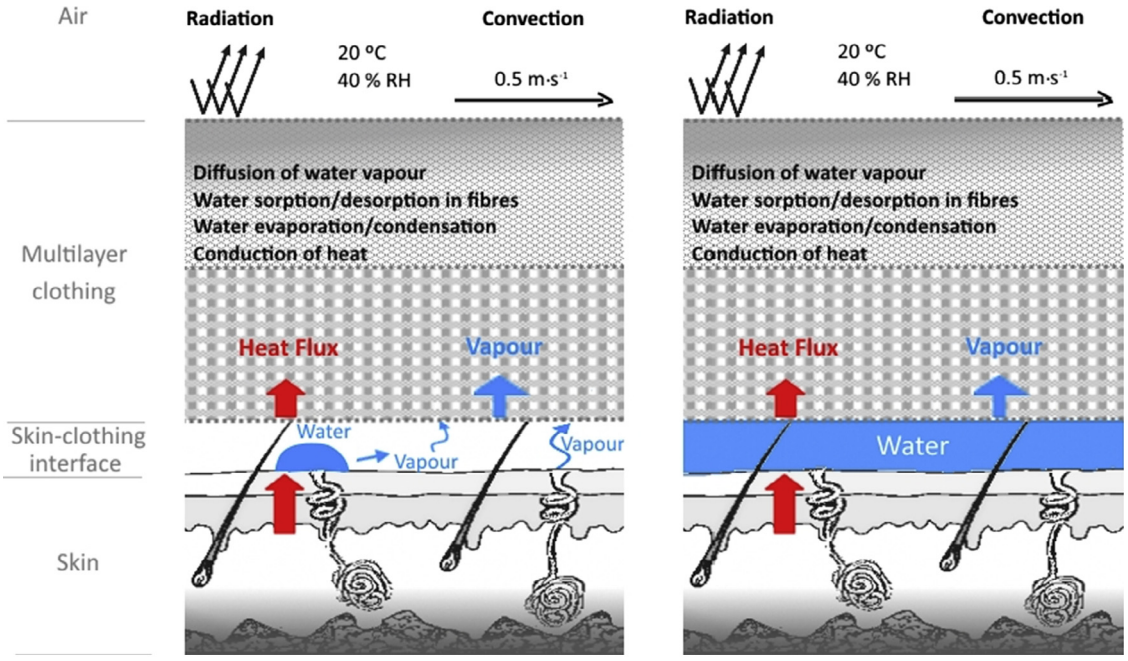

Fig. 2. Schematic diagram of a multilayer clothing facing the skin and of the surrounding environment conditions, prior and after full wetting of the skin: (a) skin not fully wet (perspiration and sweating present) and (b) skin fully wet (only sweating).

sorbed in fibres immediately becomes in equilibrium with the water vapour inside the textile pores.

Four textile elements were assembled in terms of volume fraction: a fraction of fibre (ε_{ds}; considered constant [36]), a fraction of water bounded in the fibre (ε_{bw}), a fraction of free water (ε_1), and finally a fraction of gas inside the textile pores (air + water vapour; ε_γ). These fractions are related by:

$$\varepsilon_{ds} + \varepsilon_{bw} + \varepsilon_l + \varepsilon_\gamma = 1 \tag{2.1}$$

Two energy balances were set, one for the gaseous phase (Eq. (2.2)) and another for the solid phase (Eq. (2.3)).

$$\varepsilon_\gamma \cdot \rho_\gamma \cdot C_{p_\gamma} \cdot \frac{\partial T}{\partial t} + \frac{\partial}{\partial x}\left(-\varepsilon_\gamma \cdot k_\gamma \cdot \frac{\partial T}{\partial x}\right) + a_s \cdot h_c \cdot (T - T_f) = 0 \tag{2.2}$$

$$\begin{aligned}&\left(\varepsilon_{bw} \cdot \rho_w \cdot C_{p_w} + \varepsilon_{ds} \cdot \rho_{ds} \cdot C_{p_{ds}} + \varepsilon_L \cdot \rho_L \cdot C_{p_L}\right) \cdot \frac{\partial T_f}{\partial t} \\ &+ \frac{\partial}{\partial x}\left(-[\varepsilon_{bw} + \varepsilon_{ds} + \varepsilon_L] \cdot k_\sigma \cdot \frac{\partial T_f}{\partial x}\right) + \Delta h_{vap} \cdot (\dot{m}_{LG} - \dot{m}_{GS}) \\ &- \Delta h_{sorp} \cdot (\dot{m}_{GS} + \dot{m}_{LS}) - a_s \cdot h_c \cdot (T - T_f) = 0\end{aligned} \tag{2.3}$$

In the energy balance to the gaseous phase (Eq. (2.2)), the first and second terms represent, respectively, the accumulation and conduction of energy through the textile thickness, and the third term the convective exchange of energy between the gas and the surface of the fibres. In the energy balance to the solid phase (Eq. (2.3)), the first, second and fifth terms represent the accumulation, conduction, and heat exchange between the solid and the gaseous phases, respectively, while the third takes into account the energy associated with water phase change and the fourth the energy associated with water sorption in the fibres.

The thermal conductivity of the solid phase (k_σ) is given by [37],

$$k_\sigma = \frac{k_w \cdot \rho_w \cdot (\varepsilon_{bw} + \varepsilon_l) + k_{ds} \cdot \rho_{ds} \cdot \varepsilon_{ds}}{\rho_w \cdot (\varepsilon_{bw} + \varepsilon_l) + \rho_{ds} \cdot \varepsilon_{ds}} \tag{2.4}$$

and the gas thermal conductivity (k_γ) by,

$$k_\gamma = \frac{k_v \cdot \rho_v + k_a \cdot \rho_a}{\rho_v + \rho_a} \tag{2.5}$$

where the density, specific heat, and thermal conductivity of water and fibre (subscripts *w* and *ds*, respectively) can be found in literature [38], while the volume fractions of fibre, bounded water, and gas depend on the textile structure and on the type of material. To determine these parameters, the experimental procedures reported in Neves et al. [24] were used. More properties of the gaseous phase such as the gas specific heat (Cp_γ), gas pressure (p_γ), air partial pressure (p_a), water vapour partial pressure (p_v), dry air density (ρ_a), and gas density (ρ_γ) are described by Eqs. (2.6)(2.10).

$$Cp_\gamma = \frac{Cp_a \cdot \rho_a + Cp_v \cdot \rho_v}{\rho_\gamma} \tag{2.6}$$

$$p_a = p_\gamma - p_v \tag{2.7}$$

$$p_v = \frac{\rho_v \cdot R \cdot T}{M_{H_2O}} \tag{2.8}$$

$$\rho_a = \frac{p_a \cdot M_a}{R \cdot T} \tag{2.9}$$

$$\rho_\gamma = \rho_a + \rho_v \tag{2.10}$$

The equations expressing the enthalpies of water sorption in the fibre and of water vaporisation (Δh_{sorp} and Δh_{vap}, respectively) can be found in literature [38,39].

The fibre regain, which is related with the fibre affinity with water, is the ratio between the mass of water retained in the fibre and the mass of dry fibre [40]. The instantaneous and equilibrium regains ($Regain_t$ and $Regain_{eq}$, respectively), are expressed by Eqs. (2.11) and (2.12), respectively [39]. The equilibrium regain of most materials depends on the relative humidity and is nearly the same

at different temperatures if the ambient relative humidity is the same [39].

$$Regain_t = \frac{\varepsilon_{bw} \cdot \rho_w}{\varepsilon_{ds} \cdot \rho_{ds}} \tag{2.11}$$

$$Regain_{eq} = 0.578 \cdot Regain_{f(\varphi=65\%)} \cdot \varphi \cdot [(0.321 + \varphi)^{-1} + (1.262 - \varphi)^{-1}] \tag{2.12}$$

The source term due to vapour sorption ($\Delta h_{sorp} \cdot \dot{m}_{GS}$, Eq. (2.3)) was modelled assuming that the diffusion is instantaneous [24]:

$$\dot{m}_{GS} = \frac{16 \cdot D_f \cdot \varepsilon_{ds} \cdot \rho_{ds}}{d_f^2} \cdot (Regain_t - Regain_{eq}) \tag{2.13}$$

where the ratio between the diffusivity of water in fibres (D_f) and the square diameter of fibre (d_f^2) is a sorption rate factor which considers the actual fibre/yarn shape and size distribution. This ratio is usually chosen to fit the experimental data [24,37].

Inside textile pores, water can exist in both states: liquid and vapour. The rate of condensation of water vapour is given by Eq. (2.14) (for temperatures lower than the saturation temperature) whereas the rate of evaporation is given by Eq. (2.15) (for temperatures higher than the saturation temperature).

$$\dot{m}_{LG} = k_c^{cond} \cdot a_s \cdot (\rho_v - \rho_v^{sat}) \quad \text{if} [T < T^{sat} \text{ and } \rho_v > \rho_v^{sat}] \tag{2.14}$$

$$\dot{m}_{LG} = k_c^{evap} \cdot a_s \cdot (\rho_v^{sat} - \rho_v) \cdot f_A \quad \text{if} [T \geqslant T^{sat} \text{ and } \rho_v \leqslant \rho_v^{sat}] \tag{2.15}$$

Condensation (Eq. (2.14)) occurs on the full surface of the fibre whereas evaporation (Eq. (2.15)) occurs only on the portion of the fibre surface covered by liquid, f_A. Further considerations that support Eqs. (2.14) and (2.15) are shown in Appendix A.

The continuity equation in the textile (Eq. (2.16)) accounts for the water accumulation inside the pores of textile (first term), the water vapour diffusion along textile thickness (second term), and the water accumulated inside and sorbed on the fibres surface (third and fourth terms).

$$\frac{\partial(\varepsilon_\gamma \cdot \rho_v)}{\partial t} + \frac{\partial}{\partial x}\left(-D_{ef}\frac{\partial \rho_v}{\partial x}\right) = \dot{m}_{LG} - \dot{m}_{GS} \tag{2.16}$$

The effective diffusivity of gas through the textile (D_{ef}, Eq. (2.17)) can be related to the gas fraction (ε_γ), the diffusivity of water vapour in air (D_a, Eq. (2.18); [39,41]), and the tortuosity of the textile (τ),

$$D_{ef} = \frac{\varepsilon_\gamma \cdot D_a}{\tau} \tag{2.17}$$

where D_a is calculated as,

$$D_a\ [m^2 \cdot s^{-1}] = 2.23 \times 10^{-5} \cdot \left(\frac{T}{273.15}\right)^{1.75} \tag{2.18}$$

The effective diffusivity of gas was calculated (Eq. (2.17)) using values of gas fraction and tortuosity based on the specific characteristics of the textile, in order to obtain a realistic estimate of effective diffusivity. For that purpose, the gas fraction and textile tortuosity were obtained via experimental procedures [24]. The gas fraction was related with the textile variables obtained under constant temperature and humidity conditions: the fraction of fibre, the fraction of bounded water (via isothermal sorption curve, [40]) and the effective density of the textile [24]. The tortuosity was also obtained under equilibrium conditions, however, through tests of evaporative resistance [24].

In the continuity equation of the water retained in the fibres (Eq. (2.19)), one considered the accumulation in the fibres (first term), the water vapour sorbed on the fibres surfaces ($\dot{m}_{GS}$, Eq. (2.14) and (2.15)), and the free water ($\dot{m}_{LS}$, Eq. (2.20)).

$$\rho_w \frac{\partial \varepsilon_{bw}}{\partial t} = \dot{m}_{GS} + \dot{m}_{LS} \tag{2.19}$$

where $\dot{m}_{LS}$ is calculated as follows,

$$\dot{m}_{LS} = 16 \cdot \frac{D_f}{d_f^2} \cdot \varepsilon_{ds} \cdot \rho_{ds} \cdot (Regain_{eq} - Regain_t) \cdot f_A \tag{2.20}$$

The previous equation is reported in the literature in an equivalent form [36]. The advantage of Eq. (2.20) is that it only requires the estimation of two parameters (i.e. D_f and d_f) instead of three ([36]; see Appendix B).

The continuity equation of free water in the textile pores is given by Eq. (2.21).

$$\rho_w \cdot \frac{\partial \varepsilon_l}{\partial t} = -(\dot{m}_{LS} + \dot{m}_{LG}) \tag{2.21}$$

2.2. Boundary conditions and numerical procedure

The one dimensional model considers the transport along the thickness of the multilayer clothing, i.e. from the boundary facing the skin to the boundary exposed to the environment (Fig. 2). The boundary condition at the surface facing the skin was defined according to the user activity level (Fig. 1), i.e. based on the changes occurring at the skin. In the first phase (acclimatization period; phase 0, Fig. 1) one considered that the temperature and perspiration rate at the skin were constant, i.e. 34 °C (Dirichlet condition) and 9 g m^{-3} h^{-1} (Neumann condition), respectively. Moreover, at $t = 0$, the multilayer clothing was assumed in equilibrium with the mentioned skin conditions and with the environment temperature and relative humidity. The exercise phase (phase I, Fig. 1) was described at the boundary facing the skin, by a sweating rate of 240 g m^{-3} h^{-1} and a heat flux of 139 W m^{-2}. The latter value considers that, from the energy produced by the body (300 W m^{-2}; [42]), a portion is used to evaporate sweat (161 W m^{-2} corresponding to the evaporation of 240 g m^{-3} h^{-1}) and the rest is effectively transferred to the clothing layers (139 W m^{-2}). The post-exercise phase (phase II, Fig. 1) was described by a perspiration rate of 9 g m^{-3} h^{-1} (equivalent to insensible perspiration) and a heat flux of 59 W m^{-2} (difference between the heat released by the body, 65 W m^{-2} [43], and that used to evaporate 9 g m^{-3} h^{-1} of water, i.e. 6 W m^{-2}).

A Neumann boundary condition for heat and mass transfer was considered at the clothing surface exposed to the environment (Fig. 2). The heat was assumed to be released to the environment by convection and radiation (Eqs. (2.22) and (2.23)) and the water vapour by convection (Eq. (2.24)).

$$h_c^{conv} \cdot (T_{amb} - T)_{x=L} = -\varepsilon_\gamma \cdot k_\gamma \left.\frac{\partial T}{\partial x}\right|_{x=L} \tag{2.22}$$

$$h_c^{conv} \cdot (T_{amb} - T_f)_{x=L} + \varepsilon_r \cdot \sigma \cdot (T_{amb}^4 - T_f^4)_{x=L} = -(\varepsilon_{bw} + \varepsilon_{ds} + \varepsilon_l) \cdot k_\sigma \cdot \left.\frac{\partial T_f}{\partial x}\right|_{x=L} \tag{2.23}$$

$$k_c^{conv} \cdot (\rho_{amb} - \rho_v)_{x=L} = -D_{ef} \left.\frac{\partial \rho_v}{\partial x}\right|_{x=L} \tag{2.24}$$

In the previous equations, h_c^{conv} is the convective heat transfer coefficient, k_c^{conv} the convective mass transfer coefficient, T_{amb} the ambient temperature, and ρ_{amb} the ambient concentration of water vapour. The convective heat transfer coefficient was calculated assuming that the clothing is covering a human torso (similar to experimental procedures carried out with torso manikins; [12]),

and the air flows perpendicular to the torso surface. Accordingly, the Nusselt number (Nu) is given by Eq. (2.25) (valid for $Re{\cdot}Pr > 0.2$; [44]).

$$\mathrm{Nu} = \frac{h_c^{conv} \cdot d_{torso}}{k_a} = 0.3 + \frac{0.62 \cdot Re^{1/2} \cdot Pr^{1/3}}{[1 + (0.4/Pr)]^{1/4}} \cdot \left[1 + \left(\frac{Re}{282,000}\right)^{5/8}\right]^{4/5} \quad (2.25)$$

In Eq. (2.25), the Reynolds number (Re) was calculated assuming an air velocity of 0.5 m s^{-1} (to mimic conditions in standardised thermal insulation testing, e.g. ISO 15831 [45]) and a Prandtl number (Pr) evaluated at the film temperature (27 °C; [46]). The torso diameter (d_{torso}) and the air conductivity (k_a) were set to 0.3 m [12] and 2.6 × 10^{-2} W m^{-1} K^{-1} [46], respectively. Therefore, by solving Eq. (2.25), a h_c^{conv} of 4.5 W m^{-2} K^{-1} was obtained. A convective mass transfer coefficient (k_c^{conv}) of 3.9 × 10^{-3} m s^{-1} was then obtained following the Lewis expression (2.26; [44]).

$$k_c^{conv} = \frac{h_c^{conv}}{\rho_a \cdot C_a \cdot L_e^{2/3}} \quad (2.26)$$

A finite element approach was used to solve the governing equations: energy conservation in gaseous and solid phases (Eqs. (2.2) and (2.3), respectively), mass transfer in textile (Eq. (2.16)), free water accumulation in pores (Eq. (2.21)), and water retention in fibres (Eq. (2.19)). The water sorption rates in fibres, from gas and free water, were calculated through Eqs. (2.13) and (2.20), respectively. When there was any free water in the textile, the evaporation or condensation water rates were calculated by Eq. (2.15) or Eq. (2.14), respectively.

In the numerical procedure, a second order discretization scheme, a time-step of 0.01 s, and a maximum number of mesh elements of 1400 (found adequate to ensure grid-independent results) were used.

3. Numerical simulation of heat and mass transfer through multilayer clothing

The present model was implemented and its numerical predictions were compared to experimental temperature and humidity data obtained during evaporative resistance tests [24]. Following validation (Section 3.1), the model was used (Section 3.2) to study the effect of several properties of multilayer clothing, for different heat/sweat release (mimicking different exercise intensity).

3.1. Model validation

3.1.1. Experimental approach

The accuracy of the model described in Section 2 was evaluated by comparison of numerical predictions and experimental data, obtained during evaporative resistance tests, of two textiles samples (Table 1). During the tests, the temperature and humidity in the middle of the samples were continuously measured (more details in [24]).

The textile sample was initially in equilibrium with the ambient temperature and water vapour content (considering 35 °C and 40% RH). The sample was placed inside a sweating guarded hotplate ([24,47]) which exposed it to a humidity gradient at isothermal conditions: the surface facing the apparatus plate was exposed to a saturated current of water vapour (RH = 100%, at 35 °C), while the other surface was exposed to a constant air flow (1 m s^{-1}) at 35 °C and 40% RH [24]. These test conditions follow those described in the evaporative resistance tests standard [47].

3.1.2. Numerical assumptions

In the 1D model, the following boundary conditions were considered: a Dirichlet boundary condition for heat and mass transfer, at the surface facing the plate (i.e. constant plate temperature and relative humidity; Table 1) and a Neumann boundary condition at the surface exposed to the ambient air (i.e. convective mass and heat transfer coefficients: 0.01 m s^{-1} and 12.6 W m^{-2} K^{-1}, respectively; [24]). At the beginning of the test ($t = 0$), the temperature along the textile thickness (i.e. in gaseous and solid phases) was considered uniform (T_0 in Table 1), while the water content in the fibres (i.e. in solid phase) was considered in equilibrium with the humidity of the gaseous phase (φ_0 in Table 1). The governing energy and mass conservation equations were then solved for the entire numerical domain, as described in Section 2.2.

3.1.3. Comparison between experimental data and numerical predictions of temperature and relative humidity

Fig. 3 shows measured and predicted transient temperature and relative humidity data for each textile sample (at the middle plane of the samples; Table 1). At the beginning of the test ($t = 0$) each sample was exposed to a humidity gradient across its structure [24,47]. This gradient induced the diffusion of water vapour through the sample, and the corresponding increase of the relative humidity in the pores (Fig. 3a and b). After that, the water content and the water sorption rate in the fibres increased and, consequently, there was a release of energy and an initial increase of temperature (Fig. 3a). For example, after 3 min, the most hydrophilic textile (i.e. wool; sample A, Fig. 3a) shows a temperature of 38.7 °C, i.e. 5 °C above its initial temperature. Over time, the relative humidity profile tends to a new equilibrium value (Fig. 3b) and the rate of water sorption diminishes, reducing the energy release and, thus, the temperature in the middle of the sample (Fig. 3a). Over the test period, this temperature tends to the ambient temperature (i.e. 35 °C).

The experimental and numerical results shown in Fig. 3 are in good agreement. As expected, the higher deviations occur at the initial moments of the tests, as a result of the higher variations of the water vapour partial pressure and of the saturation vapour pressure. The maximum deviation in relative humidity occurs for sample B during the first minute of test, with a predicted relative humidity 4.2 percentage points lower than the corresponding experimental value (Sample B, Fig. 3b). The temperature predictions show a maximum deviation of 0.7 °C for sample B (Fig. 3a). These consistent results indicate that the transient model predictions are accurate, and so, can be used to study heat and mass transfer across textiles.

The developed model was used to analyse the influence of clothing and fibres properties on the temperature at the skin-facing boundary and on water content inside clothing, for different rates of heat/sweat release (mimicking different levels of exercise intensity). As reference for clothing materials, the characteristics and properties of the textiles used to validate the numerical model were used (Table 1). The main results of this analysis are discussed in the following section.

3.2. Influence of several parameters/characteristic of multilayer clothing on its thermal performance

Before the preparation of a clothing prototype, its characteristics and properties can be studied in order to maximise its thermal performance and minimise moisture accumulation within its layers (that may be associated, for instance, to chilling discomfort in sportswear [18], or changes in thermal performance of firefighter's protective garments [36]). This study aims to clarify how clothing materials affect the temperature and water content of the clothing surface in contact with the skin.

Table 1
Properties of water, air, gas, and textiles samples defined in numerical simulations.

Observation	Parameter	Unit	Value	Source
Water, air, and gas properties	Cp_v	J kg^{-1} K^{-1}	1862	Ref. [46]
	Cp_w	J kg^{-1} K^{-1}	4190	Ref. [46]
	Cp_a	J kg^{-1} K^{-1}	1003	Ref. [46]
	ρ_w	kg m^{-3}	1000	Ref. [46]
	k_w	W K^{-1} m^{-1}	0.60	Ref. [46]
	M_{H2O}	kg mol^{-1}	18.02×10^{-3}	Ref. [46]
	k_a	W K^{-1} m^{-1}	2.56×10^{-2}	Ref. [46]
	M_a	kg mol^{-1}	28.97×10^{-3}	Ref. [46]
	k_v	W K^{-1} m^{-1}	2.46×10^{-2}	Ref. [46]
	R	J K^{-1} mol^{-1}	8.314	Ref. [46]
	φ_{plate}	–	1.00	Experimental; Ref. [24]
	T_{plate}	K	308.15	Experimental; Ref. [24]
Sample A [layer A]	k_{ds}	W K^{-1} m^{-1}	0.20	Ref. [38]
	Cp_{ds}	J kg^{-1} K^{-1}	1360	Ref. [38]
	ρ_{ds}	kg m^{-3}	1300	Ref. [38]
	$Regain_f$	–	0.15	Ref. [38]
	D_f	s^{-1}	4.5×10^{-14}	Fit
	d_f	m	24×10^{-6}	Estimated
	L	m	8.57×10^{-3}	Experimental; Ref. [24]
	ε_{ds}	–	0.069	Experimental; Ref. [24]
	τ	–	1.18	Experimental; Ref. [24]
	h_c	W K^{-1} m^{-2}	2.88	Fit
	T_0	K	306.85	Experimental; Ref. [24]
	φ_0	–	0.35	Experimental; Ref. [24]
Sample B [layer B]	k_{ds}	W K^{-1} m^{-1}	0.18	Weighted average, Ref. [38]
	Cp_{ds}	J kg^{-1} K^{-1}	1285	Weighted average, Ref. [38]
	ρ_{ds}	kg m^{-3}	1425	Weighted average, Ref. [38]
	$Regain_f$	–	0.11	Weighted average, Ref. [38]
	D_f	s^{-1}	4.3×10^{-14}	Fit
	d_f	m	24×10^{-6}	Estimated
	L	m	6.00×10^{-3}	Experimental; Ref. [24]
	ε_{ds}	–	0.116	Experimental; Ref. [24]
	τ	–	1.24	Experimental; Ref. [24]
	h_c	W K^{-1} m^{-2}	2.88	Fit
	T_0	K	306.75	Experimental; Ref. [24]
	φ_0	–	0.36	Experimental; Ref. [24]

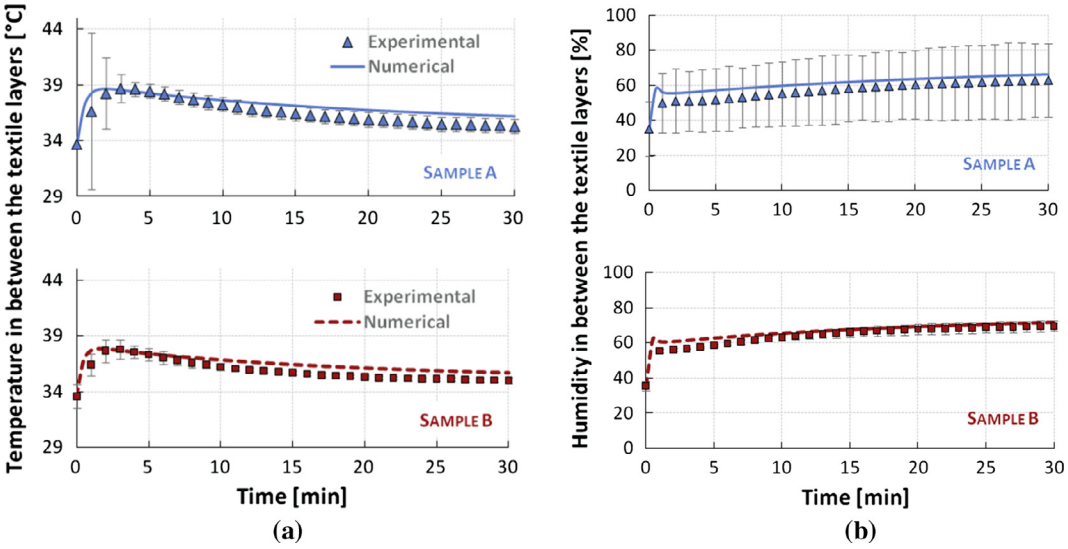

Fig. 3. Experimental and numerical data obtained in the middle plane of samples A and B [24] as a function of time; (a) temperature and (b) relative humidity (two independent measurements for sample A; three independent measurements for sample B; 95% confidence interval).

In this study, the effects of several characteristics and properties of multilayer clothing (and of its fibres) on heat and mass transport through its porous layers were analysed, for different levels of heat/sweat release (Fig. 1). The clothing has two layers, one facing the skin (layer A, Table 1) and another exposed to the environment (layer B, Table 1). Two different types of hygroscopic textiles were selected: wool and a mixture of wool and cotton (layer A and B, respectively; Table 1), with different physical properties (e.g. tortuosity and fraction of fibre). The general characteristics of the garment, such as the thickness and emissivity of the outer surface of the clothing (i.e. the surface exposed to environment) were set 1 mm and 0.7 [48–50], respectively. To analyse independently

the effect of each clothing property on the transport rates, each property was assumed to change relative to what is shown in Table 1, while the remaining were taken as given in the table.

During the exercise phase (Fig. 1), the boundary conditions at the skin (i.e. sweat rate and heat flux) were changed, affecting the clothing properties (e.g. thermal insulation and evaporative resistance), in particular near the surface facing the skin. This ultimately influences the wearer thermal exchange. For that reason, focus was put in the surface facing the skin, analysing how a change in the clothing (and fibres) properties affects the skin temperature and the water content in the multilayer clothing.

Several parameters influence the heat and mass transfer through clothing. The fibre fraction and the path tortuosity influence the diffusion of water vapour from the skin to the ambient while the thermal conductivity of the fibres affects the heat transport rates. The effects of these parameters were studied by changing, independently, the value of each parameter within the range shown in Table 2. Particular attention was put on the parameters/properties of clothing inner layer (i.e. layer A, Table 2), because it is in contact with the skin, and thus, is often very relevant for the wearer thermal exchange. Moreover, the effect of the surface emissivity of the clothing outer layer (i.e. layer B, Table 2) was also evaluated. The ranges considered in the analyses included values that are typical of textile materials (taken from literature) but also less common possibilities (e.g. regain values as high as 0.30 [39,51], or density values of 7850 kg m^{-3} [52] that are typical of ferrous metals), which enabled the study of different possibilities in terms of materials. Therefore, the possibility of using new materials to manufacture clothing was explored, which could result in products with improved thermal performance and/or new functionalities.

Fig. 4 shows the influence of the fibre fraction of the inner layer, on the numerical predictions obtained at the clothing inner surface (i.e. clothing surface facing the skin), during the exercise and post-exercise phases (Fig. 1). The fibre fraction affects properties related to water vapour transport, such as the effective diffusivity of water vapour through the clothing structure (Eq. (2.17)), the amount of water retained in the fibres (Eqs. (2.11) and (2.12)), and the water sorption rates from the water vapour and from the free water (Eqs. (2.13) and (2.20), respectively). During the exercise phase (first 30 min), an increase of the fibre fraction implies an augment in the water sorption rate in the fibres (Fig. 4a), and consequently, an increase of the fraction of bounded water (Fig. 4b). The increase in water sorption rate implies that more water vapour is removed from the clothing pores and more energy is released, as a result of vapour condensation and water sorption in fibres. Therefore, the relative humidity decreases and the temperature increases with the increasing fibre fraction (Fig. 4c and d, respectively). For example, at the time the maximum temperature occurs, the change in the fibre fraction (of clothing inner layer) from 7% to 40% leads to a decrease of 17 percentage points in relative humidity (from 67.7 to 50.9%) and an increase of 0.4 °C in temperature (Fig. 4c and d, respectively). During the exercise phase, the water content tends to a new value of equilibrium (as water sorption rate in fibres tends to zero, Fig. 4a). After 30 min of exercise, the inner layer with lower fibre fraction (7%) shows values of water content and temperature very near those at equilibrium (1.8% and 34.1 °C, respectively). At the same instant, the surface temperature of the inner layer with higher fibre fraction (40%) is still decreasing while the fraction of bounded water is still increasing (Fig. 4d and b, respectively). In equilibrium (phase I), this layer shows a surface temperature and a fraction of bounded water of 32.3 °C and 11.7%, respectively.

When the post-exercise phase starts (after 30 min, Fig. 4), the heat flux and sweating rate at the skin are reduced (phase II, Fig. 1), and consequently, the temperature and relative humidity in the pores at the inner surface of clothing decrease (Fig. 4d and c, respectively). Therefore, the water is desorbed from the fibres to the pores (negative water sorption rate, Fig. 4a) and the fraction of bounded water decreases (Fig. 4d).

At the beginning of the post-exercise phase, the inner layer with fibre fraction of 40% has more water retained in fibres (Fig. 4b). Therefore, the gradient of water concentration between the fibres and the gaseous phase and, thus, the water desorption rate, is higher than for the layer with fibre fraction of 7% (negative water sorption rate, Fig. 4a). Thus, the fraction of water retained in the fibres decreases at a higher rate (Fig. 4d). For example, from 30 to 60 min, the fraction of bounded water diminishes approximately 2.0 and 0.7 percentage points for the inner layer with fibre fractions of 40% and 7%, respectively. During this period, the retained water desorbs from fibres and is vaporised, removing thermal energy from the system. Therefore, the layer showing the higher water desorption rates (fibre fraction of 40%; negative water sorption rates, Fig. 4a) also shows the lowest temperature (throughout the post-exercise phase, Fig. 4d). At 60 min, a 5.7-fold increase in the fibre fraction (from 7 to 40%) implies a decrease of 1.5 °C in the temperature of the inner layer surface. This effect is opposed to that observed during the first minutes of exercise (where higher fibre fractions imply higher temperature, Fig. 4d). This opposite trend occurs due to sorption and desorption phenomena that occur during the exercise and post-exercise phases, respectively. When these phenomena have a significant influence in the heat transferred trough clothing, the properties that affect the water sorption (desorption) rate and the water retention in the fibres determine an opposite effect on both phases of exercise.

The results shown in Fig. 4 demonstrate that the inner layers with higher fibre fractions imply lower temperature during the post-exercise phase and more water retained during both exercise and post-exercise phases. This may affect the tactile comfort perception and potentiate problems such as increased skin irritation (because of friction) or excessive cooling of the body. Thus, from this point-of-view, manufacturers should prefer a clothing inner layer with a low fraction of fibre.

Table 2
Properties of multilayer clothing (layer A facing the skin and layer B facing the environment) and fibres considered in the study.

Observation	Parameter	Units	Range
Layer A	Fraction of fibre	–	[0.07,0.40]
	Tortuosity[a]	–	[1.2,3.0]
Fibres of layer A	Fibre regain	$kg_{H2O}\ kg_{fibre}^{-1}$	[0.07,0.30]
	Fibre thermal conductivity	$W\ m^{-1}\ K^{-1}$	[0.1,0.3]
	Fibre density	$kg\ m^{-3}$	[910,7850]
	Coefficient of water diffusion in fibres	$m^2\ s^{-1}$	$[4 \times 10^{-16}, 4 \times 10^{-11}]$
	Specific heat[a]	$J\ kg^{-1}\ K^{-1}$	[200,1430]
Surface of layer B	Emissivity	–	[0.1,0.9]

[a] No significant influence on inner surface temperature and water content of clothing.

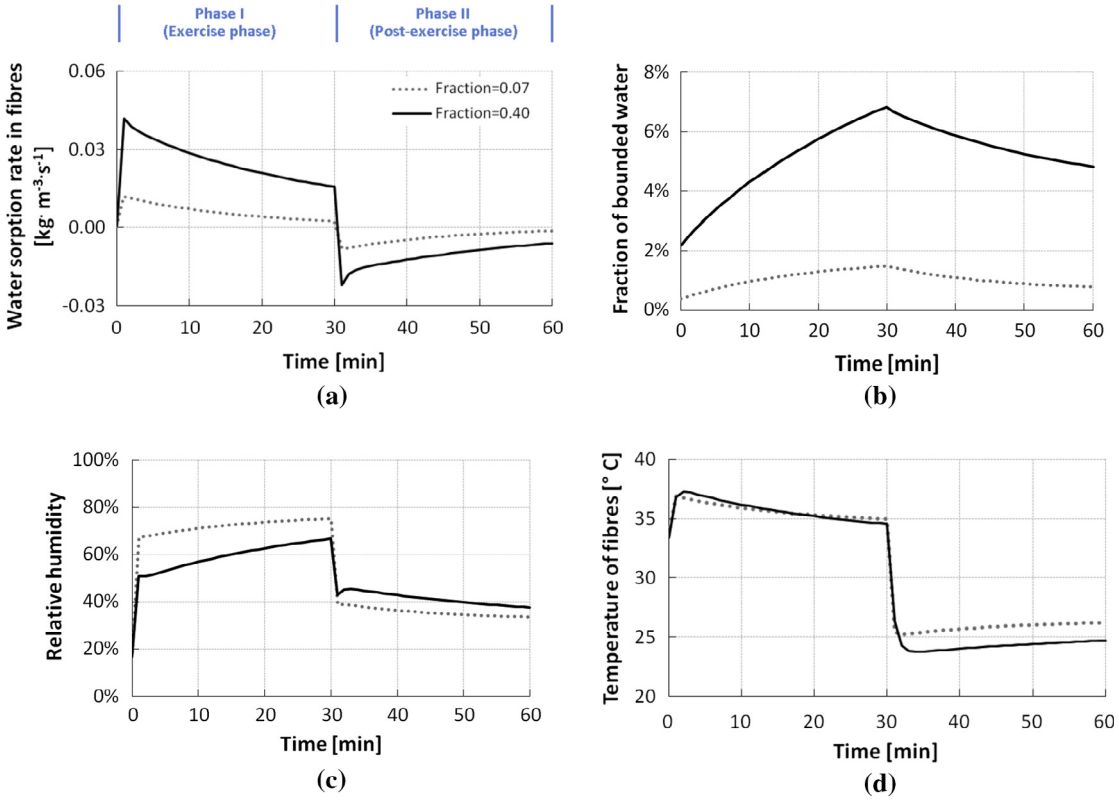

Fig. 4. Influence of the fibre fraction of the clothing inner layer on numerical predictions obtained at the clothing inner surface, during the exercise and post-exercise phases (Fig. 1); (a) water sorption rate in fibres; (b) fraction of bounded water; (c) relative humidity, and; (d) temperature of the fibres.

Similar analyses were conducted for all the properties of clothing mentioned in Table 2. The obtained results were then compiled (Fig. 5) in order to allow an easy understanding of the different effects. This Figure shows the influence of clothing (and fibres) properties on temperature and on fraction of bounded water at the inner surface of clothing (surface facing the skin), during activities with different intensities (Fig. 1). This influence is quantified by deviations in temperature and fraction of bounded water, when the value of a given property is increased according to the ranges given in Table 2. These quantifications were done at three instants: (1) at the moment when the maximum temperature is achieved (Fig. 5a); (2) at the end of the exercise phase (phase I, Fig. 1; 30 min, Fig. 5b); and (3) at the end of the post-exercise phase (phase II, Fig. 1; 60 min, Fig. 5c). The results obtained for the fibre fraction (showed in Fig. 4) were also included in Fig. 5.

The fibre regain is a direct indicator of its affinity to water. A change in this parameter can be seen as a change of the hygroscopic properties of the fibres, or a change in the type of fibre. This parameter, like the fraction of fibre, also affects significantly the clothing water content (Fig. 5a and b). Fig. 5a shows that a 5.7-fold increase in the fibre fraction (from 7 to 40%) and a 4.3-fold increase in the regain of the fibres (from 0.07 to 0.30) implies respectively a 6.0 and 4.1-fold increase in the fraction of bounded water. This occurs because both parameters influence the amount of water retained in the fibres (Eqs. (2.11) and (2.12)) and also the water sorption rates from the water vapour and from the free water (Eqs. (2.13) and (2.20), respectively). The same effect is observed for the post-exercise phase, i.e. at 60 min (Fig. 5b), when the wearer heat flux and the sweat rate were reduced (Fig. 1).

The thermal conductivity of the fibres influences the thermal conductivity of the textile solid phase (Eq. (2.4)) and the thermal energy transferred by conduction (second term, Eq. (2.3)). As a result, the skin temperature is affected by altering the fibre thermal conductivity (Fig. 5). For example, a 3-fold increase in the fibre thermal conductivity leads to a decrease of 2.7 °C (Fig. 5a) in the maximum skin temperature and a decrease of 1.5 °C in skin temperature at the end of exercise phase (Fig. 5b). The same trend is observed at the end of post-exercise phase (Fig. 5c): a 3-fold increase in the fibre conductivity leads to a decrease of 0.9 °C in the skin temperature. Furthermore, Fig. 5 shows that for the range considered in this work, the fibre thermal conductivity has no significant effect on the water content of the inner layer.

The density of the fibre has also significant influence on the water content of the inner layer (Fig. 5). The density of the fibres influences the energy balance of the solid phase (Eq. (2.3)), the amount of water retained in the fibres (Eq. (2.11)) as well as the sorption rates of water vapour and of free water in the fibres (Eqs. (2.13) and (2.20), respectively). An increase of the fibre density from 910 to 7850 kg m^{-3} (8.6-fold increase) implies a 8.7-fold increase (from 0.3 to 2.8%) in the fraction of bounded water when the temperature achieves the maximum value (Fig. 5a), and a 6.5-fold increase (from 1.1 to 6.9%) after 30 min of exercise (Fig. 5b). At 60 min (Fig. 5b), an augment of 6940 kg m^{-3} in the fibre density, of 33 percentage points in the fibre fraction (from 7 to 40%), and of 23 percentage points in the regain of fibres (from 0.07 to 0.30) lead respectively to a 9.2-, 6.2-, and 4.5-fold increase in the fraction of bounded water. Because these increases in water content near the skin could imply problems like skin irritation during exercise (due to increased clothing friction) or may affect the tactile comfort perception, it is advisable to minimise the fraction of retained water near the skin, i.e. in the inner clothing layer. In summary, the results in Fig. 5 reveal that, to reduce the water content in the inner clothing layer, the fibres should have low density, reduced regain (or hydrophilicity), and low fraction of fibre. To adjust the density or regain of fibres, different materials can be used. In this regard, one should mention that although the use of different types of fibres could influence the textile tortuosity (i.e. the complexity of the porous network), we observed that the tortuosity (tested in

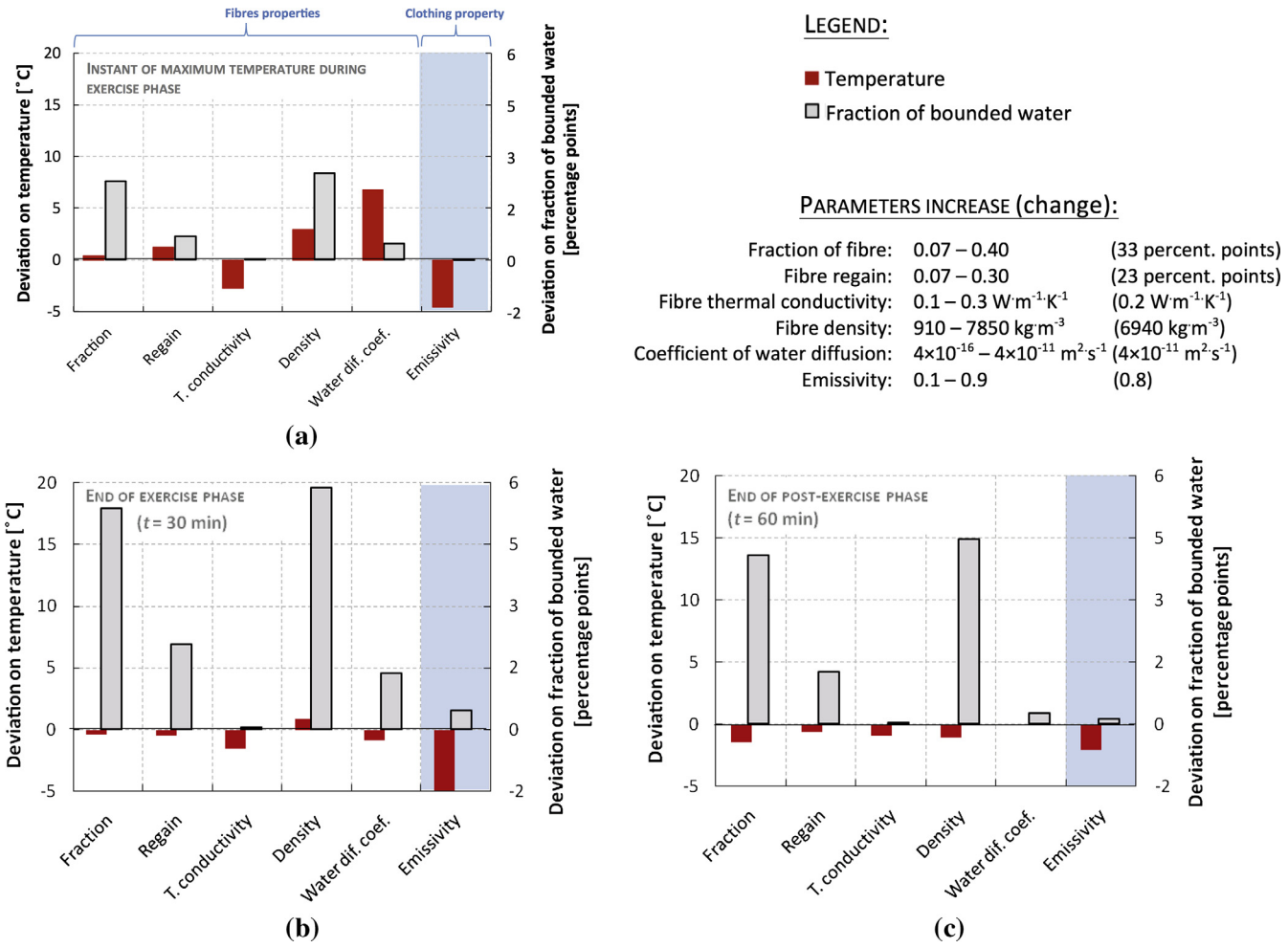

Fig. 5. Influence of an increase of clothing and fibres parameters (values range shown in Table 2) on temperature and on fraction of bounded water in the inner surface of clothing, during the exercise and post-exercise phases (Fig. 1); (a) when the maximum temperature is achieved; (b) at the end of exercise phase (30 min), and; (c) at the end of post-exercise phase (60 min).

the range 1.3–3.0, Table 2), has no significant effect on the skin temperature and on the water content of the inner layer.

The water diffusion coefficient in the fibres significantly affects the temperature in the inner surface of clothing during the exercise phase (Fig. 5a). This coefficient influences the water sorption rate in the fibres (Eq. (2.13)), and, therefore, an increase in this parameter leads to higher values of maximum temperature and fraction of bounded water, during the first minutes of exercise (positive deviation in Fig. 5a). In this period, an increase of the coefficient from 4×10^{-16} to 4×10^{-11} $m^2 s^{-1}$, leads to an increase of 6.8 °C in the surface temperature and a 2.2-fold augment in the fraction of bounded water (from 0.4 to 0.8%, Fig. 5a). However, after 30 min (Fig. 5b), the fibres with higher coefficient show the lowest skin temperature (negative deviation of 0.8 °C). The reason for this is straightforward: higher water diffusion coefficient implies higher rates of sorption/desorption (Eq. (2.13)), and consequently, the equilibrium is established faster. For that reason, at the end of exercise phase (30 min, Fig. 1), a 4.4-fold increase in the fraction of bounded water is obtained for the fibres with the higher water diffusion coefficient (Fig. 5b).

The emissivity of the clothing outer surface significantly affects, as expected, the skin temperature during both exercise and post-exercise phases (Fig. 5). Higher values of emissivity imply more heat transfer by radiation between the clothing and the environment, and, consequently, a lower temperature at the skin surface (negative deviation, Fig. 5a). For example, an augment in the emissivity of the outer surface from 0.1 to 0.9 implies a decrease of 4.5 °C in the maximum temperature and of 4.9 °C in the temperature at the end of the exercise phase (Fig. 5a and b, respectively). This dependency is consistent with results reported in literature [17,31], though, in addition to previous works, the approach implemented in this work also takes into account the coupling between heat and mass transfer along the clothing structure. For instance, at the end of the exercise and post-exercise phases (phase I and II, Fig. 1), the mentioned increase in emissivity leads respectively to a 1.4 and 1.2-fold increase in the fraction of bounded water near the skin (Fig. 5b).

In general, during the exercise phase (Fig. 5a and b), the emissivity of the outer surface and the coefficient of water diffusion in the fibres affect considerably the temperature of the inner layer. At the same time, the fraction of bounded water in the inner surface of the clothing (Fig. 5a and b) is significantly affected by the fraction of fibre, density of the fibre, regain/hydrophilicity, and coefficient of water diffusion in the fibres. At the end of post-exercise phase (Fig. 5c), the parameters that significantly affect the water content at the inner layer are the fraction of fibre, density, and regain/ hydrophilicity of fibres.

4. Conclusions

Numerical simulations were conducted to analyse the effect of several textiles characteristics (the outer surface emissivity,

tortuosity, and fraction of fibre) and fibre properties (affinity with water, coefficient of water diffusion in the fibres, thermal conductivity, density, and specific heat) on heat and mass transfer across multilayer clothing, during physical activities with different intensities (i.e. heat/sweat release). Model validation was performed against experimental data obtained during measurements of textile evaporative resistance.

During the exercise phase, the results obtained show that an increase in the coefficient of water diffusion in the fibre and an increase in its hygroscopic nature increase the maximum skin temperature and the water content in the textile layer facing the skin, respectively. In the post-exercise phase, textiles with high fraction of fibres, regain/hydrophilicity, and density of fibres retain more water. To reduce the water content near the skin, the less hydrophilic layer should face the skin and the more hydrophilic layer should face the ambient. Moreover, the results show that a change in the emissivity of the clothing outer surface has substantial influence on the evolution of the skin temperature, during the exercise and post-exercise phases. On the other hand, properties such as textile tortuosity and specific heat of the fibres do not show a significant effect on the transport rates through clothing.

The numerical approach described allows the study of the effects of different properties, which are difficult to control accurately in experiments (because the change of a parameter often causes the change of others). The obtained results can assist manufacturers and clothing developers to identify clothing properties that can be adjusted to optimise the apparel thermal performance, the water accumulation/distribution within clothing layers, and the associated tactile comfort perception.

Our results highlight the advantage of studying numerically the heat and mass transfer in clothing products (e.g. of protective clothing or sports apparel) as a way to optimise its thermal performance, while reducing the number of prototypes and cycles of product development.

Acknowledgements

The support provided by Fundação para a Ciência e a Tecnologia (FCT), Portugal under grant number SFRH/BDE/51382/2011 is gratefully acknowledged.

Appendix A. Mass rates of condensation and evaporation of water

Inside textile pores, when water vapour concentration is greater than the saturation concentration, the water vapour condenses at the entire surface of fibres. Thus the mass transfer area corresponds to the total area of the fibres [34]. The water condensation rate ($\dot{m}_{cond}$) is therefore proportional to the specific surface area of the fibre (a_s) and to the difference between the vapour concentration in the gas (ρ_v), and vapour concentration near the surface where condensation occurs (ρ_v^{sat}),

$$\dot{m}_{cond} = k_c^{cond} \cdot a_s \cdot (\rho_v - \rho_v^{sat}) \tag{A.1}$$

where k_c^{cond} is the mass transfer coefficient of condensation. The specific surface area of the fibre is the ratio between the surface area of the fibre (A_{ds}) and the total volume of the textile (V_T),

$$a_s = \frac{A_{ds}}{V_T} \tag{A.2}$$

During evaporation, the mass transfer area corresponds to the area covered by liquid water (A_l),

$$a_s^* = \frac{A_l}{V_T} = \left(\frac{A_{ds}}{V_T}\right) \cdot \left(\frac{A_l}{A_{ds}}\right) = a_s \cdot f_A \tag{A.3}$$

therefore, the evaporation rate can be calculated as,

$$\dot{m}_{evap} = k_c^{evap} \cdot a_s \cdot f_A \cdot (\rho_v^{sat} - \rho_v) \tag{A.4}$$

The fraction f_A was determined by the following equation,

$$f_A = \frac{\varepsilon_l}{\varepsilon_l^{cri}} = \left(\frac{V_l/V_T}{V_l^{cri}/V_T}\right) = \left(\frac{A_l \cdot L_l/V_T}{A_l \cdot L_l/V_T}\right) = \left(\frac{A_l}{A_{ds}}\right) \tag{A.5}$$

where ε_l is liquid water fraction and ϵ_L^{cri} is the liquid water fraction at the critical limit corresponding to the situation in which the mass transfer area is equal to the total area of the fibre (A_{ds}) and also 10% of the pores are occupied by liquid water (a value of 10% was proposed in Ref. [53] in the absence of any better experimental data; $\epsilon_L^{cri} = 0.1 \times \{1 - \varepsilon_{ds}\}$). Fig. 6 exemplifies the fibre area covered by liquid water as function of f_A.

Consider a fibre diameter d_f, with only a portion of the surface covered by liquid water (area A_l; in blue in Fig. 6a). Assuming that the water film is very thin, the evaporation area is comparable to the fibre area covered by water, A_l. As the water concentration in pores increases, the fibre surface covered by water also increases until it reaches a critical limit, when the water covers the entire surface of the fibre (Fig. 6b). In this situation, if more water condensates, it becomes mobile (Fig. 6c; scenario not considered in the implemented model). Furthermore, if the film thickness is considered small, the evaporation area can be assumed equal to the surface area of the fibre, A_{ds}.

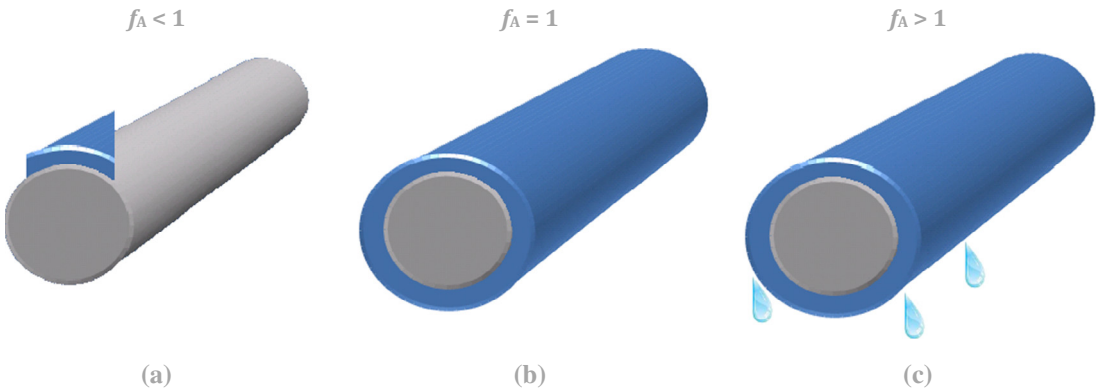

Fig. 6. Fibre (gray) covered by liquid water (blue) for different fractions of area covered by liquid water (f_A).

Appendix B. Equivalent expressions to calculate the mass rate sorption of free water in fibres

Considering that the water diffuses through the fibres radius (r), the mass rate sorption of free water in fibres ($\dot{m}_{LS}$) can be expressed by:

$$\frac{1}{r}\frac{d}{dr}\left(r\cdot(-D_f)\frac{dC_f}{dr}\right)=-\dot{m}_{LS} \tag{B.1}$$

This equation can be integrated taking the following boundary conditions:

$$\left.\frac{dC_f}{dr}\right|_{r=0}=0, C_f(R_f)=C_{feq} \quad \text{and} \quad C_f(0)=C_f,$$

Furthermore, by replacing the water concentration in the fibres by the fibre regain, the following equation for the mass rate of free water sorption in fibres is obtained,

$$\dot{m}_{LS}=\frac{16\cdot D_f\cdot\varepsilon_{ds}\cdot\rho_{ds}}{d_f^2}\cdot(Regain_{eq}-Regain_t) \tag{B.2}$$

The Eq. (B.2) considers that the mass transfer area is equal to the total area of the fibre surface. However, the model assumes that only part of the fibre area is covered by free water (Appendix A) and therefore the right side of B.2 equation must be multiplied by the fraction f_A

$$\dot{m}_{LS}=\frac{16\cdot D_f\cdot\varepsilon_{ds}\cdot\rho_{ds}}{d_f^2}\cdot(Regain_{eq}-Regain_t)\cdot f_A \tag{B.3}$$

The Eq. (B.3) is apparently different from the equation reported in literature (Eq. (B.4); [36]),

$$\dot{m}_{LS}=k_c^{ls}\cdot a_s\cdot\gamma_{ls}\cdot\left(\frac{Regain_{eq}}{Regain_t}-1\right)\cdot f_A \tag{B.4}$$

However, (B.3) and (B.4) are equivalent, as demonstrated below,

$$\begin{aligned}\dot{m}_{LS}&=\frac{16\cdot D_f}{d_f^2}\cdot\varepsilon_{ds}\cdot\rho_{ds}\cdot(Regain_{eq}-Regain_t\cdot)f_A\\&=4\cdot4\cdot\frac{D_f}{d_f}\cdot\frac{\varepsilon_{ds}}{d_f}\cdot\rho_{ds}\cdot Regain_t\cdot\left(\frac{Regain_{eq}}{Regain_t}-1\right)\cdot f_A\\&=\left[\frac{D_f}{d_f}\right]\cdot\left[4\cdot\frac{\varepsilon_{ds}}{d_f}\right]\cdot[4\cdot\rho_{ds}\cdot Regain_t]\cdot\left(\frac{Regain_{eq}}{Regain_t}-1\right)\cdot f_A\\&\quad\Updownarrow\qquad\Updownarrow\qquad\Updownarrow\\&\quad k_c^{ls}\qquad a_s\qquad\gamma_{ls}\\&=k_c^{ls}\cdot a_s\cdot\gamma_{ls}\cdot\left(\frac{Regain_{eq}}{Regain_t}-1\right)\cdot f_A\end{aligned} \tag{B.5}$$

References

[1] E.W. Rosenberg, H. Blank, S. Resnik, Sweating and water loss through the skin, J. A. M. A. 179 (1962) 809–811.

[2] H. Tokura, M. Shimomoto, T. Tsurutani, T. Ohta, Circadian variation of insensible perspiration in man, Int. J. Biometeorol. 22 (1978) 271–278. http://www.ncbi.nlm.nih.gov/pubmed/750507.

[3] F.G. Benedict, C.G. Benedict, The nature of the insensible perspiration, Proc. Natl. Acad. Sci. U.S.A. (1927) 364–369.

[4] A. Melikov, T. Ivanova, G. Stefanova, Seat headrest-incorporated personalized ventilation: thermal comfort and inhaled air quality, Build. Environ. 47 (2012) 100–108, http://dx.doi.org/10.1016/j.buildenv.2011.07.013.

[5] A. Alahmer, A. Mayyas, A.A. Mayyas, M.A. Omar, D. Shan, Vehicular thermal comfort models; a comprehensive review, Appl. Therm. Eng. 31 (2011) 995–1002, http://dx.doi.org/10.1016/j.applthermaleng.2010.12.004.

[6] M. Zhao, C. Gao, F. Wang, K. Kuklane, I. Holmér, J. Li, A study on local cooling of garments with ventilation fans and openings placed at different torso sites, Int. J. Ind. Ergon. 43 (2013) 232–237, http://dx.doi.org/10.1016/j.ergon.2013.01.001.

[7] A. Psikuta, K. Kuklane, A. Bogdan, G. Havenith, S. Annaheim, R.M. Rossi, Opportunities and constraints of presently used thermal manikins when used for simulation of the human body, Int. J. Biometeorol. (2015), http://dx.doi.org/10.1007/s00484-015-1041-7.

[8] F. Wang, G. Havenith, T.S. Mayor, K. Kuklane, J. Léonard, M. Zwolinska, S. Hodder, C. Wong, J. Kishino, X. Dai, Clothing real evaporative resistance determined by means of a sweating thermal manikin: a new round-robin study, in: Sci. Conf. Smart Funct. Text. Well-Being, Therm. Comf. Clothing, Des. Therm. Manikins Model. (Ambience14 10i3m), Tampere, Finland, 2014.

[9] G. Song, S. Paskaluk, R. Sati, E.M. Crown, J. Doug Dale, M. Ackerman, Thermal protective performance of protective clothing used for low radiant heat protection, Text. Res. J. 81 (2010) 311–323, http://dx.doi.org/10.1177/0040517510380108.

[10] E.B. Elabbassi, S. Delanaud, K. Chardon, J.-P. Libert, V. Candas, Electrically heated blanket in neonatal care: assessment of the reduction of dry heat loss from a thermal manikin, Environ. Ergon. 3 (2005) 431–435, http://dx.doi.org/10.1016/S1572-347X(05)80068-0.

[11] C. Keiser, Moisture Management in Firefighter Protective Clothing, Swiss Federal Institute of Technology, 2007.

[12] A. Psikuta, Development of an "Artificial Human" for Clothing Research, De Montfort University Leicester, 2009.

[13] J. Yang, W. Weng, M. Fu, Coupling of a thermal sweating manikin and a thermal model for simulating human thermal response, Procedia Eng. 84 (2014) 893–897, http://dx.doi.org/10.1016/j.proeng.2014.10.512.

[14] L. Wang, Y.-C. Chang, Y.-C. Shih, The evaluation of moisture management fabrics, in: Fiber Soc. 2012 Spring Conf., 2012, p. 32.

[15] S.F. Neves, J.B.L.M. Campos, T.S. Mayor, Numerical simulation study on the heat and mass transfer through multi-layer textile assemblies, in: COMSOL Conf. 2012 Milan, 2012.

[16] X. Yin, Q. Chen, N. Pan, A more comprehensive transport model for multilayer-cloth for perspiration based infrared camouflage, Appl. Therm. Eng. 68 (2014) 10–19, http://dx.doi.org/10.1016/j.applthermaleng.2014.04.007.

[17] S. Couto, J.B.L.M. Campos, T.S. Mayor, On the performance of a mitt heating multilayer: a numerical study, Int. J. Cloth. Sci. Technol. 23 (2011) 373–387, http://dx.doi.org/10.1108/09556221111166301.

[18] H. Wu, J. Fan, Study of heat and moisture transfer within multi-layer clothing assemblies consisting of different types of battings, Int. J. Therm. Sci. 47 (2008) 641–647, http://dx.doi.org/10.1016/j.ijthermalsci.2007.04.008.

[19] P. Gibson, Modeling heat and mass transfer from fabric-covered cylinders, J. Eng. Fiber. Fabr. 4 (2009) 1–8.

[20] S.F. Neves, J.B.L.M. Campos, T.S. Mayor, A numerical simulation study on the thermal performance of ventilated clothes, in: 6th Eur. Conf. Prot. Cloth., Bruges, Belgium, 2014.

[21] X. Yin, Q. Chen, N. Pan, Feasibility of perspiration based infrared Camouflage, Appl. Therm. Eng. 36 (2012) 32–38, http://dx.doi.org/10.1016/j.applthermaleng.2011.12.001.

[22] O. Neiva, F.T. Pinho, T.S. Mayor, A numerical study on the cooling power of an enhanced convection solution for footwear, in: Japan-Portugal Nano-Biomedical Eng. Symp., Bragança, Portugal, 2011, p. 2.

[23] S.F. Neves, S. Couto, J.B.L.M. Campos, T.S. Mayor, Advances in the optimisation of apparel heating products: a numerical approach to study heat transport through a blanket with an embedded smart heating system, Appl. Therm. Eng. 87 (2015) 491–498, http://dx.doi.org/10.1016/j.applthermaleng.2015.05.035.

[24] S.F. Neves, J.B.L.M. Campos, T.S. Mayor, On the determination of parameters required for numerical studies of heat and mass transfer through textiles – Methodologies and experimental procedures, Int. J. Heat Mass Transf. 81 (2015) 272–282, http://dx.doi.org/10.1016/j.ijheatmasstransfer.2014.09.038.

[25] B. Liu, K. Min, J. Song, Effect of thermal plume on personal thermal comfort in displacement ventilation at one side of the room, in: 9th Int. Symp. Heating, Vent. Air Cond. 3rd Int. Conf. Build. Energy Environ., Elsevier B.V., 2015, pp. 1058–1066, http://dx.doi.org/10.1016/j.proeng.2015.09.103.

[26] N. Gao, J. Niu, CFD study on micro-environment around human body and personalized ventilation, Build. Environ. 39 (2004) 795–805, http://dx.doi.org/10.1016/j.buildenv.2004.01.026.

[27] D. Sørensen, Modelling flow and heat transfer around a seated human body by computational fluid dynamics, Build. Environ. 38 (2003) 753–762, http://dx.doi.org/10.1016/S0360-1323(03)00027-1.

[28] M. Salmanzadeh, G. Zahedi, G. Ahmadi, D.R. Marr, M. Glauser, Computational modeling of effects of thermal plume adjacent to the body on the indoor airflow and particle transport, J. Aerosol Sci. 53 (2012) 29–39, http://dx.doi.org/10.1016/j.jaerosci.2012.05.005.

[29] R. Rocha, O. Neiva, J.B.L.M. Campos, F.T. Pinho, T.S. Mayor, A cooling solution for footwear - numerical analysis, in: Fiber Soc. 2012 Spring Conf. – Fiber Res. Tomorrow's Appl., St. Gallen, Switzerland, 2012, pp. 230–231.

[30] T.S. Mayor, S. Couto, A. Psikuta, R. Rossi, A numerical analysis on the transport phenomena across horizontal clothing microclimates, in: 6th Eur. Conf. Prot. Cloth., Bruges, Belgium, 2014.

[31] T.S. Mayor, S. Couto, A. Psikuta, R. Rossi, Advanced modelling of the transport phenomena across horizontal clothing microclimates with natural convection, Int. J. Biometeorol. 59 (12) (2015) 1875–1889, http://dx.doi.org/10.1007/s00484-015-0994-x.

[32] T.S. Mayor, S. Couto, A. Psikuta, R. Rossi, Transport phenomena in clothing wavy microclimates – a numerical study, in: Sci. Conf. Smart Funct. Text. Well-Being, Therm. Comf. Clothing, Des. Therm. Manikins Model. (Ambience14 10i3m), Tampere, Finland, 2014.

[33] T.S. Mayor, D. Oliveira, R. Rossi, S. Annaheim, Numerical simulation of the transport phenomena in tilted clothing microclimates, in: XVI Int. Conf. Environ. Ergon., Portsmouth, UK, 2015.
[34] C.V. Le, N.G. Ly, R. Postle, Heat and mass transfer in the condensing flow of steam through an absorbing fibrous medium, Int. J. Heat Mass Transf. 38 (1995) 81–89, http://dx.doi.org/10.1016/0017-9310(94)00139-M.
[35] Y. Li, Z. Qingyong, K.W. Yeung, Influence of thickness and porosity on coupled heat and liquid moisture transfer in porous textiles, Text. Res. J. 72 (2002) 435–446, http://dx.doi.org/10.1177/004051750207200511.
[36] R.L. Barker, G. Song, H. Hamouda, D.B. Thompson, A.V. Kuznetsov, A.S. Deaton, P. Chitrphiromsri, Modeling of Thermal Protection Outfits for Fire Exposures F01-NS50, North Caroline State, 2004.
[37] P. Gibson, Multiphase Heat and Mass Transfer Through Hygroscopic Porous Media With Applications to Clothing Materials, Massachusetts, 1996.
[38] P. Gibson, M. Charmchi, The use of volume-averaging techniques to predict temperature transients due to water vapor sorption in hygroscopic porous polymer materials, J. Appl. Polym. Sci. 64 (1997) 493–505.
[39] N. Pan, P. Gibson, Thermal and Moisture Transport in Fibrous Materials, first ed., Wookhead Publishing Limited, 2006.
[40] W.E. Morton, W.S. Hearle, Physical Properties of Textile Fibres, fourth ed., Woodhead Publishing Limited, 2008.
[41] B.E. Poling, J.M. Prausnitz, J.P. O'Connel, The properties of gases and liquids, fifth edit, McGraw Hill, 2001, http://dx.doi.org/10.1036/0070116822.
[42] I. American Society of Heating, Refrigerating and Air-Conditioning Engineers, Ashrae ® Handbook - Fundamentals, Inch-pound, 2009.
[43] K. Parsons, Human Thermal Environments, Taylor & Francis, Second edi, 2003.
[44] Y.A. Çengel, Natural convection, in: Heat Mass Transf. - A Prat. Approach, third edit., McGraw-Hill Science/Engineering/Math, 2007, p. 28,29,759.
[45] ISO 15831(2004) Clothing - Physiological effects -Measurement of a thermal manikin, in: 1st edn, International Organization of Standardization (ISO), Geneva, 2004.
[46] M.W. Haynes, D.R. Lide, Handbook of Chemistry and Physics, (n.d.) 6-15-20. http://www.hbcpnetbase.com/ (accessed 09.09.12).
[47] ISO 11092:1993(E) - Textiles - Physiological effects - Measurement of thermal and water-vapour resistance under steady-state conditions (sweating guarded-hotplate test), 1993.
[48] D. Ding, T. Tang, G. Song, A. MacDonald, Characterizing the performance of a single-layer fabric system through a heat and mass transfer model - Part II: Thermal and evaporative resistances, Text. Res. J. 81 (2011) 945–958, http://dx.doi.org/10.1177/0040517510395994.
[49] D. Ding, T. Tang, G. Song, A. MacDonald, Characterizing the performance of a single-layer fabric system through a heat and mass transfer model - Part I: Heat and mass transfer model, Text. Res. J. 81 (2010) 398–411, http://dx.doi.org/10.1177/0040517510388547.
[50] A. Ghazy, Air Gap in Protective Clothing During Flash Fire Exposure, University of Saskatchewan, 2011.
[51] P.W. Gibson, M. Charmchi, Modeling convection/diffusion processes in porous textiles with inclusion of humidity-dependent air permeability, Int. Commun. Heat Mass Transf. 24 (1997) 709–724, http://dx.doi.org/10.1016/S0735-1933(97)00056-0.
[52] J.H. Lienhard IV, J.H. Lienhard V, A Heat Transfer Textbook, third ed., Phlogiston Press, Cambridge Massachusetts, 2006, http://dx.doi.org/10.1115/1.3246887.
[53] M. Sozen, K. Vafai, Analysis of the non-thermal equilibrium condensing flow of a gas through a packed bed, Int. J. Heat Mass Transf. 33 (1990) 1247–1261, http://dx.doi.org/10.1016/0017-9310(90)90255-S.